KINEMATICS OF THE CENTRAL REGIONS OF NGC 1672

R. Díaz,[1,2] G. Carranza,[1,3] H. Dottori,[4] AND G. Goldes[1,3]

ABSTRACT

We present the detailed velocity field of the central 2 kpc of the LINER galaxy NGC 1672. The iso-velocity map shows a rotational pattern with a velocity gradient of 50 km s^{-1} arcsec^{-1} in the inner 6″ (1″ ≈ 70 pc), indicating a mass of ≈9 × 10^8 $M_\odot$ inside a radius of 125 pc, equivalent to a density of ≈2 × 10^{11} $M_\odot$ kpc^{-3}. It also shows some asymmetries on a larger scale. An offset of ≈60 pc between the nuclear continuum barycenter and the kinematical center is also found. Satoh's model fitting to the observed velocity field reveals several nonaxisymmetric residuals, which do not correlate well with the bar or the circumnuclear ring of H II regions. The inner rotation curve of NGC 1672 reveals that the circumnuclear ring of star formation is located on an inner Lindblad resonance (ILR), and not near the peak of the Lindblad curve, $\Omega - (\kappa/2)$, as suggested by previous works, which also claimed that the ring rotates faster than its ambient. This motion is not confirmed by the two-dimensional residual-velocity map.

Subject headings: galaxies: active — galaxies: individual (NGC 1672) —
galaxies: kinematics and dynamics — galaxies: nuclei

1. INTRODUCTION

NGC 1672 is a southern barred spiral galaxy that presents a circumnuclear ring of star formation (Sersic & Pastoriza 1965) surrounding a nucleus with low-level activity (Verón-Cetty & Verón 1986). Circumnuclear rings of star formation have been revealed in a number of galaxies with active nuclei (Arribas & Mediavilla 1993; Genzel et al. 1995). These rings seem to be located close to the turnover points of the rotation curves (Telesco & Decher 1988; Dottori 1990), and the turnover points are closer to the nuclei than in normal galaxies (Storchi-Bergmann, Wilson, & Stone 1996, hereafter SBWB), suggesting that galaxies with circumnuclear rings of star formation have a higher central mass concentration than normal spirals. The numerical study of gas dynamics in barred spirals has shown that it is plausible to associate ringlike concentrations of gas with the presence of dynamical resonances between orbital motions and the pattern speed of a bar distortion (Combes & Gerin 1985). Otherwise, the presence of strong gaseous inflows are associated with inner Lindblad resonances (ILR) in barred galaxies (Simkin, Su, & Schwarz 1980; Athanasoula 1992a).

Active galaxies also present other peculiarities, such as several dynamically distinct systems of ionized gas, and even displacements between the mass centroid and the kinematic center (Wilson et al. 1991; Arribas, Mediavilla, & Garcia-Lorenzo 1996; Mediavilla & Arribas 1993). The small number of published nuclear velocity fields available makes it difficult to study these anomalies systematically.

NGC 1672 presents all the ingredients that favor the scenario described above. Furthermore, its distance (with a projected scale of 73 pc arcsec^{-1}, $H = 75$ km s^{-1} arcsec^{-1}) and favorable inclination of ≈40°, make this galaxy suit-

able for studying the two-dimensional velocity field around the nucleus. In this paper we present new spectroscopic data, which, analyzed together with already published data, allow us to study with high precision the behavior of the emitting gas in the central 2 kpc of this galaxy.

2. OBSERVATIONS AND DATA REDUCTION

2.1. The Instrument

The new data presented in this paper were obtained in 1995 and 1996 with the Multifunctional Integral Field Spectrograph (MIFiS) installed on the f/21 Nasmyth focus of the 60 inch telescope at Bosque Alegre Station of the Cordoba Astronomical Observatory (a twin of the Oak Ridge telescope, Washington University); a description of the MIFiS is given by Díaz et al. (1995). The MIFiS consists of a 600 mm focal length (f/12) Maksutov-type collimator system and a 200 mm focal length (f/3.5) apochromatic camera lens. The whole system has an equivalent focal length of 10.38 m and a scale of 0″.38 pixel^{-1} with the CCD described below. The direct mode gives field images of 5′.7 × 5′.7. The detector is a CCD camera (Photometrics AT 200), with a Thomson CH 7896 1024 × 1025 chip.

2.2. Observations and Data Reduction

MIFiS was used in 1995 February and 1996 January, in the direct-image and long-slit modes (Table 1). In the long-slit mode we used a 1200 groove mm^{-1} grating in first order, giving a sampling of 0.78 Å pixel^{-1} on the detector. We used a 1″ slit width, with an effective resolved range of ≈1.6 Å. For each slit position several 30 minute spectra were obtained, and before and after each series of spectra, at each single position, zero-order images of the slit superimposed on the galaxy were obtained. The FWHM of the star images in the zero-order images were measured, allowing us to select the best-resolved observing time (1″.4 ≤ FWHM ≤ 2″.2) for this program. The spectrophotometric standards of Stone & Baldwin (1983) were observed on photometric nights in order to obtain a mean transmission function of the system.

The reduction was accomplished with ADHOC reduction software (Marseille Observatory; Boulesteix

[1] Observatorio Astronómico de Córdoba, Universidad Nacional de Córdoba, Laprida 854, 5000 Córdoba, Argentina.

[2] FoMEC, Facultad de Matemática, Astronomía y Física, Universidad Nacional de Córdoba, Argentina.

[3] Consejo Nacional de Investigaciones Cientificas y Técnicas, Argentina.

[4] Instituto de Física, Universidade Federal do Rio Grande do Sul, CP 15051, Avenue B. Gonçalves 9500, Porto Alegre, Brazil.

TABLE 1

LOG OF OBSERVATIONS WITH THE BOSQUE ALEGRE 1.5 m TELESCOPE (MIFiS)

Slit Position	P.A. (deg)	Range (Å)	Exposure (s)	Date	Comments
… …………	…	R band	120	1995 Feb 12/13	Direct image mode. Poor seeing.[a]
8…………	160	6200–7000	2 × 1800	1995 Feb 12/13	Poor seeing
9…………	160	6200–7000	2 × 1800	1995 Feb 12/13	8″ east of nucleus. Poor seeing.
… …………	…	R band	600	1996 Jan 10/11	Direct image mode
0…………	90	6300–7100	6 × 1800	1996 Jan 10/11	…
4…………	90	6300–7100	2 × 1800	1996 Jan 10/11	8″ south of nucleus
5…………	90	6300–7100	4 × 1800	1996 Jan 11/12	8″ north of nucleus
6…………	90	6300–7100	4 × 1800	1996 Jan 12/13	16″ north of nucleus
1…………	135	6250–7050	6 × 1800	1996 Jan 13/14	…
2…………	45	6250–7050	3 × 1800	1996 Jan 13/14	…
3…………	10	6250–7050	6 × 1800	1996 Jan 16/17	…
7…………	17	6250–7050	2 × 1800	1996 Jan 16/17	80″ east of nucleus
9…………	160	6250–7050	3000	1996 Jan 17/18	Cloudy
10 …………	32	6200–7000	1200	1996 Jan 18/19	43″ west of nucleus. Cloudy.
10 …………	32	6200–7000	4 × 1800	1996 Jan 20/21	13″ west of nucleus
11 …………	32	6200–7000	4 × 1800	1996 Jan 21/22	…
12 …………	32	6200–7000	2 × 1800	1996 Jan 21/22	94″ west of nucleus. Poor seeing.
13 …………	90	6200–7000	6 × 1800	1996 Jan 25/26	63″ south of nucleus
14 …………	160	6200–7000	3 × 1800	1996 Jan 27/28	11″ east of nucleus
… …………	…	R band	600	1996 Jan 27/28	Direct image mode
0…………	90	6200–7000	3x1800	1996 Jan 28/29	Cloudy

[a] " Poor seeing " means FWHM $\approx 2''$. Observing conditions were selected as stated in § 2.

1993). The standard techniques for two-dimensional detectors were applied for the reduction of images and spectral frames. $1''.52$ wide slices were extracted from the coadded two-dimensional frames at each slit position. These slices were wavelength calibrated and corrected for the mean transmission function of the observing run.

2.3. Line Fitting and Velocity Mapping

The instrumental width of night-sky emission lines was about 100 km s^{-1}. Gaussians were fitted interactively to the object emission lines down to 10% of the peak level, with an estimated mathematical uncertainty of ≈ 4 km s^{-1} for S/N ≥ 20 (easily reached in the inner 500 pc of the field). The mean value of several line fittings in each spectrum provides the line velocity. At some slit locations, asymmetries in the emission lines are evident, probably associated with dust extinction or the presence of several unresolved emission-line components. In order to check the importance of these asymmetries, we calculated the lines barycenter for 73 points along two slit angular positions, given by

$$\frac{\sum F_\lambda \lambda}{\sum F_\lambda} = \frac{\sum N_{counts} N_{channel}}{\sum N_{counts}} .$$

In 70 out of 73 points, the differences between barycenter and Gaussian velocities are smaller than the overall estimated uncertainty of 15 km s^{-1}. For the remaining three points, the resulting difference is larger than 30 km s^{-1}. We therefore concluded that the general shape of the velocity field and the rotation curve would not be affected by using Gaussian fitting instead of the emission-line barycenter.

In order to have accurate spatial positions for the velocity determinations in each extracted spectrum, zero-order double imagings of object plus slit before and after the spectroscopic exposures were used. We also obtained the spatial profiles along the slit of the Hα and continuum emissions, which correlate within $0''.3$ with the Hα image by SBWB. The positions of the spectral slices were finally referred to the barycenter of the nuclear continuum emission.

3. RESULTS

3.1. Velocity Map

For each slit position passing through the nucleus, the systemic velocity was determined as the mean of the external portions of the corresponding velocity curve. The resulting mean systemic velocity is 1325 ± 10 km s^{-1}. This value is consistent with the systemic velocity of the molecular gas (Bajaja et al. 1995).

Our data (254 points), together with those published by SBWB, furnished 309 points in the inner 2 kpc of NGC 1672, giving a complete coverage in the central kpc, arranged in a grid with spatial resolution of $1''.4$. Using this grid, we constructed the isovelocity map shown in Figure 1. It is worth noting that the oversampled central 4 × 4 presents strong velocity gradients, particularly in the southeast-northwest direction, where it amounts to ≈ 50 km s^{-1} arcsec^{-1}. This map also shows slightly distorted kinematical axes, a feature found in other nuclear velocity fields of active nuclei (e.g., NGC 4151; see Mediavilla, Arribas, & Rasilla 1992). Prominent features in Figure 1 are the sharp maxima located at 5″ to the southeast and northwest of nucleus, much closer to the center than in normal disk galaxies (Sofue 1996). Other bisymmetrical features are present in the form of secondary maxima and ridges.

The velocity pattern in the neighborhood of the kinematical center ($r \leq 1.1$ kpc) is predominantly rotational. The analysis of the V_r versus $\cos$ (P.A. − P.A.$_0$) relationship (where P.A. is the position angle of the radial velocity point and P.A.$_0$ is the position angle of the kinematical line of nodes) shows that the orientation of the kinematical major axis changes smoothly by several degrees from the inner to the outer disk, leaning toward the bar. The mean P.A. of the kinematical line of nodes of the nuclear velocity
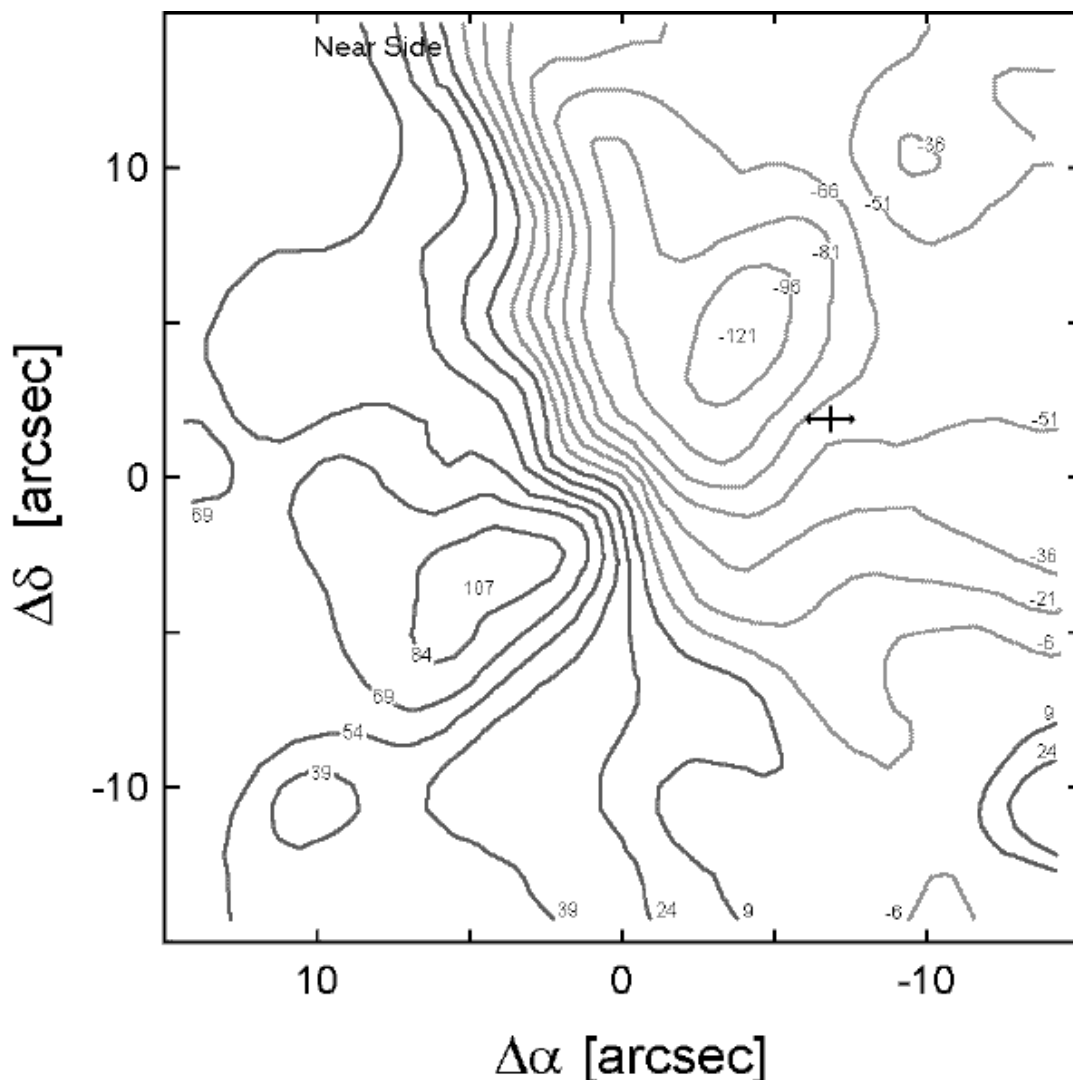
FIG. 1.—Isovelocity map generated from the grid of relative radial velocities. The near side of the galaxy is north following. The cross and the arrows indicate the center of the bar and its orientation, respectively.

field is $124° \pm 2°$, compatible with the value obtained by SBWB ($121°$ for the velocity field and $130°$ for the orientation of the inner ring), and by Sersic & Calderon (1979) ($130°$, external ring of H II regions). Other photographic determinations of this parameter for NGC 1672 are $170°$ (Tully 1988, B images) and $152°$ (Baumgart & Peterson 1986, IR images); both referred to the external disk, and the difference between these and our value (and that of SBWB as well) may indicate the presence of disk warping.

In Figure 2a we plot the circular velocity values of the central 1.5 kpc, extracted from an angular sector of $\pm 40°$ around P.A.$_0 = 124°$. The inclination value used as a first approximation for the rotation curve extraction was $36°$ (Baumgart & Peterson 1986, IR images), and the final adopted value was $40° \pm 4°$, which minimized the sum of the squares of the residual velocity values. The high dispersion of this curve does not arise from observational errors, but mainly reflects local departures from circularity. Polynomial fittings of this data show a 60 pc shift of the kinematical center toward the northwest of the geometrical center (taken here as the continuum-emission barycenter). The shift is at least 3 times higher than the positional errors

of the individual velocity determinations (§ 2). This effect is also noted in the individual radial velocity curves at different P.A. passing through the nucleus. Although it may reflect the effects of dust on the determination of the geometric center, it is worth noting that the offset nucleus (kinematical versus geometrical) is also found in other spirals galaxies (e.g., Mediavilla & Arribas 1993; Wilson et al. 1986).

3.2. Nonaxisymmetric Components of the Velocity Field

The average rotation curve of the central 2 kpc in Figure 2b was fitted with a rotation curve corresponding to Satoh's density law (Satoh 1980), which simultaneously combines a spherical and a disklike mass distribution:

$$V_c^2(R, Z) = GMR^2\{R^2 + Z^2 + a[a + 2(Z^2 + b^2)^{1/2}]\}^{-3/2} ,$$

where $V_c(R)$ is the circular velocity at position (R, Z), M is the total disk mass, and a and b are shape parameters. The fitting parameters that optimize the χ^2 test are $a = 0.078$ and $b/a = 0.5$ ($b/a \approx 1$ corresponds to a flattened disk distribution, and $b/a \approx 10$ to an ellipsoidal distribution). A Satoh's law two-dimensional radial velocity field with
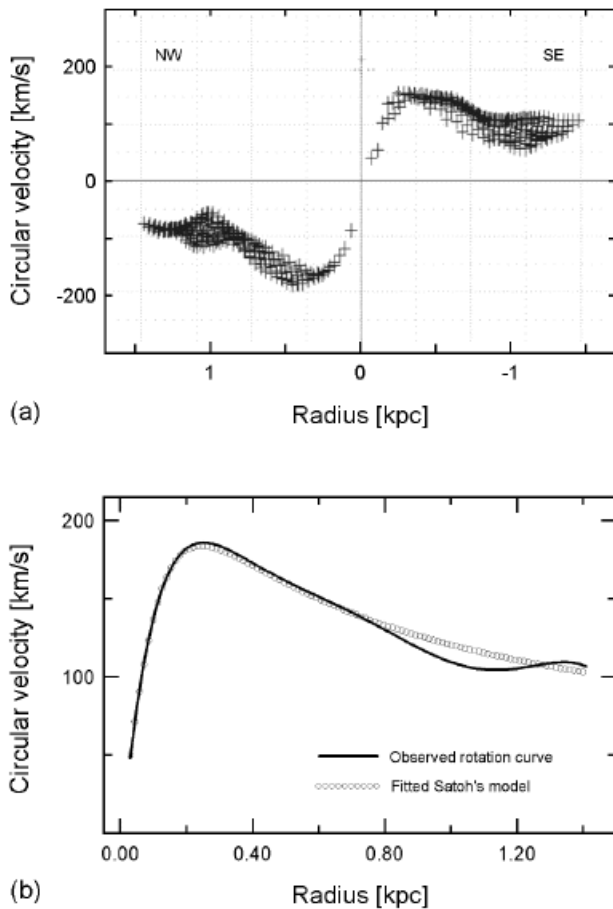
FIG. 2.—(a) Circular velocity values obtained from the velocity field, taken from an angular sector of ±40° around the kinematic line of nodes. (b) Rotation curve obtained from the set of radial velocity points inside ±40° about the kinematical line of nodes.

barred spirals by Piner, Stone, & Teuben (1995) for a galaxy with a 10 × 2.5 kpc bar (similar to NGC 1672) shows that in the central kpc, a velocity field dipolar asymmetry appears that is not aligned with the bar axis, but is probably connected to the extended bar flow. On a bit larger scale, similar to our total frame in Figure 3, Piner et al.'s model shows that noncircular asymmetries appear that are also driven by the bar nonaxisymmetric potential. Nevertheless, specific models and hydrodynamical simulations with higher central resolutions might help us to better understand the velocity residuals present in the NGC 1672 central part.

SBWB claim to have found high residual velocities associated with the circumnuclear ring of H II regions, indicating that the circumnuclear ring rotates faster than the ambient rotation (see also Storchi-Bergmann et al. 1997). In reality, the residuals they have found are a consequence of fitting a rigid body plus outer flat part model to the rotation curve, which consequently leaves the velocity curve bump (approximately located on the H II regions ring) unexplained. Satoh's potential overrides this problem, and the ring appears as a stable structure with practically pure circular motion.

3.3. Mass Distribution

The average rotation curve obtained in the previous section presents a steep slope up to the turnover, located at ≈300 pc, indicating a high mass concentration inside this region. The Keplerian mass interior to a radius of 125 pc is about $9 \pm 1 \times 10^8 \, M_\odot$, and the mass interior to the H II ring is $2.5 \pm 0.3 \times 10^9 \, M_\odot$, indicating a density of $\rho_c \approx 3 \times 10^{11} \, M_\odot \, \text{kpc}^{-3}$ for $r < 125$ pc. It is important to remark that the turnover is sharper in NGC 1672 than in other galaxies with circumnuclear rings of star formation (e.g., NGC 1097 and NGC 5248; SBWB), making the conventional fit by an inner solid body plus outer flat part rather simplistic, in the sense that the important turnover bump is ignored. In Figure 2b, such a fit would correspond to truncating the rotation curve at about 120 km s^{-1} between 150 pc $\leq r \leq$ 700 pc (see also Fig. 6 of SBWB). As a consequence, dynamical parameters derived from such models (such as the epicyclic frequency, and consequently the location of the ILR) became less accurate. The Satoh's model presented above is more flexible, and its density distribution includes an inhomogeneous bulge (Binney & Tremaine 1987):

$$\rho(R, Z) = \frac{ab^2 M}{4\pi \, S^3(Z^2 + b^2)}$$
$$\times \left[\frac{1}{(Z^2 + b^2)^{1/2}} + \frac{3}{a}\left(1 - \frac{R^2 + Z^2}{S^2}\right) \right],$$

where $S^2 = R^2 + Z^2 + a[a + 2(Z^2 + b^2)^{1/2}]$. The total mass calculated from the fit of Figure 2b in the observed region is $3.6 \times 10^9 \, M_\odot$, and the mass inside $r = 125$ pc is $7 \times 10^8 \, M_\odot$, corresponding to a density of $\rho_c \approx 2 \times 10^{11} \, M_\odot \, \text{kpc}^{-3}$, consistent with values obtained from Keplerian motion. This concentration of mass is high compared to the sample of 60 spiral galaxies of Rubin et al. (1985, and references therein), 59 of which present less steep rotation curves in the central region. From this sample, only NGC 4959, with an inner rotation curve (e.g., Kormendy 1996) similar in shape and scale (2″ ≤ r ≤ 15″) to that of NGC 1672, shows a higher central mass concentration than this galaxy.

$Z = 0$ was subtracted from the observed one, and the residual velocity field is shown in Figure 3. We identify three main lobes, A^+, B^-, and C^+, where " + " indicate redshift and " − " blueshift with respect to the axial symmetric Satoh's distribution. The lobe at the northeast (A^+) is projected onto the minor axis; since the galaxy is north precedent, the redshift is consistent with motion toward the nucleus. The other two lobes (B^- and C^+) are located on each side of the minor axis, on the farthest side of the galaxy (to the southeast). The largest blue lobe (B^-) is also consistent with motion toward the nucleus. There are four other less conspicuous velocity anomalies: D^-, D^+, E^+, and F^-. The stability of the field of residuals was tested against slight variations of the model parameters; it basically maintains these distribution and signs, although the amplitude of the central blue peak varies by ≈40% if a and a/b change by ≈10%. It is worth noting that the smallest residuals, anomalies D^- and D^+, can also be seen in the SBWB radial velocity curve along P.A. = 130° (their Fig. 10).

The observed velocity field covers more or less 15% of the bar projected size (10 × 2.9 kpc). It shows noncircular velocity residuals on 1/3 of this area. Gas flow along bars is a well-known phenomenon. Nevertheless, it is not the only noncircular motion that might exist in a barred galaxy, especially if the bar center is shifted with regard to the disk kinematical center (Colin & Athanssoula 1989), as is the case in NGC 1672. Indeed, a hydrodynamical simulation of
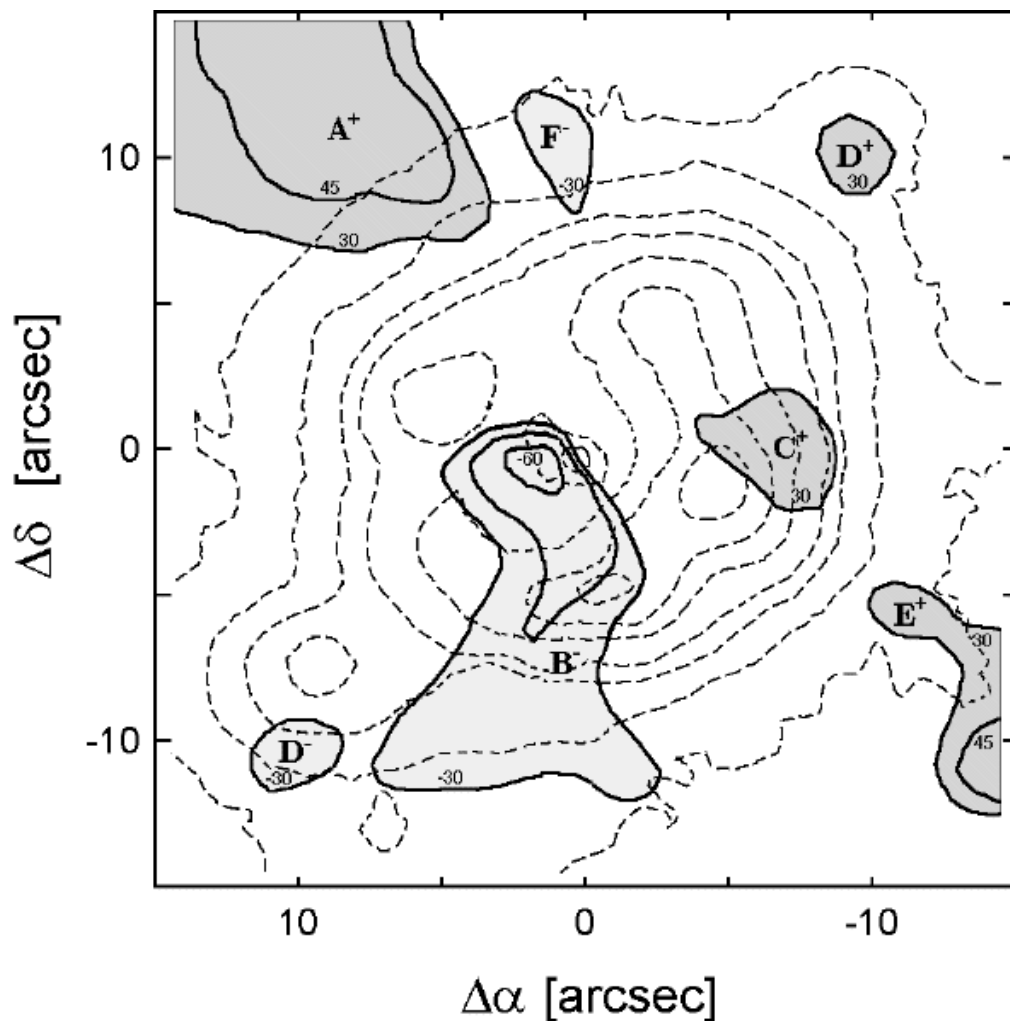
FIG. 3.—Radial velocity field residuals, obtained by subtracting a Satoh model from observations. It is superimposed on SBWB Hα isophotes (*dotted lines*).

3.4. *Inner Lindblad Resonance*

In the small number of galaxies for which an accurate rotation curve of the circumnuclear ring has been measured (e.g., NGC 7496 and NGC 4151), the ring seems to be very near to the turnover point of the rotation curve (Wilson et al. 1986; Telesco & Decher 1988). Since dynamical resonances are related to the turnover (Kormendy & Norman 1979), it is reasonable to relate circumnuclear rings to dynamical resonances. Recent hydrodynamical simulations of barred spiral galaxies (e.g., Piner et al. 1995) link the presence of a "star-forming ring" around the nucleus to a high central mass concentration, and two ILRs. In order to construct the curve $\Omega - (\kappa/2)$ for the inner regions of NGC 1672, we assume the photometric bar size ($r \approx 5.1$ kpc) given by Buta (1987), and we suppose that the corotation radius is at the end of the bar (e.g., Sparke & Sellwood 1987; Athanassoula 1992b). The resulting bar pattern angular velocity is $\Omega_b \approx 30$ km s^{-1} kpc^{-1}, which sets an ILR at $r \approx 490$ pc from the galactic center, coincident with the ring outer edge.

Although the curve has the same shape, our ILR is significantly smaller than that derived by SBWB (≈ 2 kpc). This difference is mainly due to the bulge model adopted in each case. In addition, the ring is not located on the peak of the $\Omega - (\kappa/2)$ curve, as might be inferred from Piner et al. (1995) models.

Moreover, a second ILR, although suggested by the falloff of the $\Omega - (\kappa/2)$ curve, should be located at $r < 30$ pc. Such distances from the nucleus are not reachable with either our spatial resolution or SBWB's. There is no evidence that the gas will have the same dynamical behavior at such a distance from the nucleus. Nevertheless, the unresolved nuclear Hα and [N II] 6548–6584 Å emission lines ($\langle$FWHM$\rangle \approx 300$ km s^{-1}) are broader than the corresponding H II regions lines and seem to marginally present double peaks. Higher spatial resolution and better S/N ratios would be important in order to see whether the disk extends itself inward, beyond $r \approx 30$ pc.

3.5. *Morphological Features*

In order to look for a possible association between the observed kinematical properties and some photometric features, we analyzed a combination of 10 *R*-band Johnson filter images.

Photometric profiles along and across the bar allowed us to determine that its center is shifted $\approx 2''$ to the north and $\approx 8''$ to the west of the nucleus; this means a total shift of about 600 pc to the west-northwest. Shifted bars have been
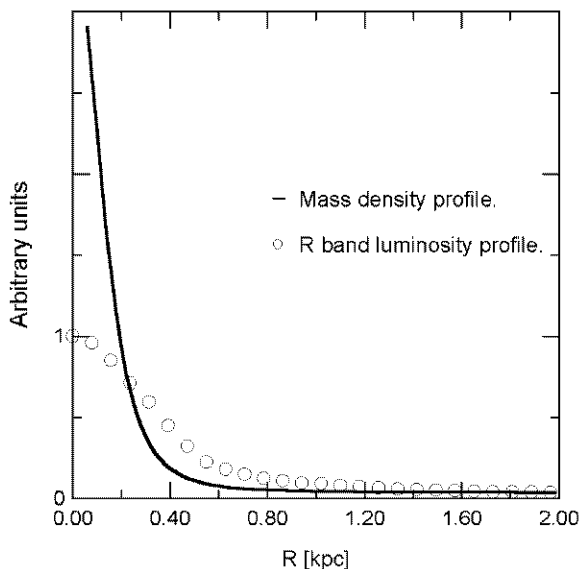
FIG. 4.—NGC 1672 central region luminosity profile compared to the Satoh model mass density profile, convolved with the night PSF. The star-forming ring extends itself approximately from 300 to 500 pc in radius.

found in other barred galaxies (Colin & Athanassoula 1981 and references therein; Dottori et al. 1996). Hydrodynamical simulations suggest that a shifted bar causes strong arm asymmetry (Colin & Athanassoula 1989), like that observed in NGC 1672.

Azimuthally averaged radial profiles of the central region of the galaxy were compared with a fitted Satoh's mass density profile (after Gaussian degradation to the level of the image resolution). Both profiles have been normalized at the outer part, and the comparison is shown in Figure 4. The relative shapes of the profiles indicate a lower $(M/L)_{red}$ on the circumnuclear ring (300 pc $\leq r \leq$ 600 pc). Inside $r \approx 300$ pc, $(M/L)_{red}$ grows to several times the value at the outer part of the observed region. This fact might be due to the presence of large amounts of obscuring dust toward the nucleus, in agreement with the strong infrared emission in this galaxy nucleus reported by De Grijp, Miley, & Lub (1987).

Anomalies D^+ and D^- are coincident with two H ɪɪ regions just outside the star-forming ring (Fig. 3). These two extensions resemble the loci at which the $x2$ family of orbits intersect the disk, as found in hydrodynamical simulations of barred galaxies (Athanassoula 1992a). This scenario is reinforced by strong dust lanes around D^+ and D^-, which characterize a strong "traffic jam" zone of interstellar material in barred galaxies (Binney & Tremaine 1987, p. 405).

The curved dust lanes of NGC 1672 (also detected with the infrared color imaging, J-K, by Regan & Vogel 1996) are leading the bar and form an angle of more than 30° with its major axis. According to the Athanassoula (1992b) and Piner et al. (1995) simulations of strong barred galaxies, it is also a consequence of the strong central mass concentration.

4. SUMMARY AND CONCLUSIONS

We present a detailed velocity field of the central 2 kpc of the LINER galaxy NGC 1672. This galaxy has a circumnuclear ring of star formation ($r \approx 350$ pc) that is located near to the turnover point of the rotation curve.

The isovelocity map shows a rotational pattern with a velocity gradient of 50 km s^{-1} arcsec^{-1} in the inner 400 pc. It also shows distorted kinematical axes. An offset of $\approx$60 pc between the nuclear continuum barycenter and the kinematical center is also found. The previously unknown inner rotation curve of this galaxy was accurately fitted with Satoh's model, composed of a strong disk and a small bulge. The residual velocity field reveals noncircular motions with an amplitude of 50–60 km s^{-1}.

Previous works have claimed that the circumnuclear ring rotates faster than its ambient, mainly because the solid body plus outer flat part model yielded strong residuals at the ring. This motion is not confirmed by our two-dimensional differential velocity map; indeed, most of the ring area has pure circular motion.

The kinematical data indicate a mass of $\approx 9 \times 10^8 \, M_\odot$ in the inner 250 pc, yielding a density of $\approx 2 \times 10^{11} \, M_\odot$ kpc^{-3}. The nuclear Hα and [N ɪɪ] 6548–6584 Å emission-line broadening is consistent with this mass concentration.

It was found that the outer edge of the circumnuclear ring of star formation coincides with an ILR located at 490 pc, closer to the center than previously estimated, indicating that circumnuclear star-forming rings do not necessarily occur at the peak of the $\Omega - (\kappa/2)$ curve.

REFERENCES

Arribas, S., & Mediavilla, E. 1993, ApJ, 410, 552
Arribas, S., Mediavilla, E., & Garcia-Lorenzo, B. 1996, ApJ, 463, 509
Athanassoula, E. 1992a, MNRAS, 259, 345
———. 1992b, MNRAS, 259, 328
Bajaja, E., Wielebinski, R., Reuter, H., Harnett, J., & Hummel, E. 1995, A&AS, 114, 147
Baumgart, C., & Peterson, C. 1986, PASP, 98, 56
Binney, J., & Tremaine, S. 1987, Galactic Dynamics (Princeton: Princeton Univ. Press)
Boulestex, J. 1993, ADHOC Reference Manual, (Marsaille: Pub. de l'Observatoire de Marseille)
Buta, R. 1987, ApJS, 64, 1
Colin, J., & Athanassoula, E. 1981, A&A, 97, 63
———. 1989, A&A, 214, 99

Combes, F., & Gerin, M. 1985, A&A, 150, 327
De Grijp, M., Miley, G., & Lub, J. 1987, A&AS, 70, 95
Díaz, R., Paolantonio, S., Goldes, G., & Carranza, G. 1995, Espectrógrafo Multifunción: Características, Puesta a Punto, Operación y Reducción de Datos (Trabajos de Astronomía ser. A) (Córdoba: National Univ. Córdoba, Fa.M.A.F)
Dottori, H. 1990, Proc. ESO-CTIO Workshop on Bulges of Galaxies 299, ed. B. Jarvis & D. Terndrup (Paris: ESO)
Dottori, H., Bica, E., Claria, J. J., & Puerari, I. 1996, ApJ, 461, 742
Genzel, R., Weitzel, L., Tacconi-Garman, L., Blietz, M., Cameron, M., Krabbe, A., Lutz, D., & Sternberg, A. 1995, ApJ, 444, 129
Kormendy, J. 1996, ApJ, 473, L91
Kormendy, J., & Norman, C. 1979, ApJ, 233, 539
Mediavilla, E., & Arribas, S. 1993, Nature, 365, 420

Mediavilla, E., Arribas, S., & Rasilla, J. 1992, ApJ, 396, 517
Piner, B., Stone, J., & Teuben, P. 1995, ApJ, 449, 508
Regan, M., & Vogel, S. 1996, in Spiral Galaxies in the Near-IR, ed. D. Minitti & H. Rix (Berlin: Springer), 269
Rubin, V., Burstein, D., Kent Ford, W., Jr., & Thonnard, N. 1985, ApJ, 289, 81
Satoh, C. 1980, PASJ, 32, 41
Sersic, J., & Calderón, J. 1979, Ap&SS, 62, 211
Sersic, J., & Pastoriza, M. 1965, PASP, 77, 287
Simkin, S., Su, H., & Schwarz, M. 1980, ApJ, 237, 404
Sofue, Y. 1996, ApJ, 458, 120

Sparke, L., & Sellwood, J. 1987, MNRAS, 225, 653
Stone, R., & Baldwin, J. 1983, MNRAS, 204, 347
Storchi-Bergmann, T., Wilson, A., & Stone, J. 1996, ApJ, 460, 252
———. 1997, ApJ, 472, 83
Telesco, G., & Decher, B. 1988, ApJ, 334, 573
Tully, R. 1988, Nearby Galaxies Catalog (Cambridge: Cambridge Univ. Press)
Véron-Cetty, M., & Véron, P. 1986, A&AS, 66, 335
Wilson, A., Baldwin, J., Sun, S., & Wright, A. 1986, ApJ, 310, 121
Wilson, A., Helfner, T., Haniff, C., & Ward, M. 1991, ApJ, 381, 79